Biochemical Pharmacology 222 (2024) 116059

Contents lists available at ScienceDirect

Biochemical Pharmacology

journal homepage: www.elsevier.com/locate/biochempharm

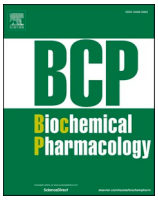

Early pharmacological profiling of isatin derivatives as potent and selective cytotoxic agents

Adrián Puerta [a], Aday González-Bakker [a], Pedro Brandão [b,c,d], Marta Pineiro [d], Anthony J. Burke [d,e], Elisa Giovannetti [f,g], Miguel X. Fernandes [h], José M. Padrón [a,*]

[a] BioLab, Instituto Universitario de Bio-Orgánica Antonio González (IUBO-AG), Universidad de La Laguna, PO Box 456, 38200 La Laguna, Spain
[b] Egas Moniz Center for Interdisciplinary Research (CiiEM), Egas Moniz School of Health & Science, 2829-511 Almada, Portugal
[c] iBB-Institute for Bioengineering and Biosciences, Department of Bioengineering, and Associate Laboratory i4HB–Institute for Health and Bio-Economy, Instituto Superior Técnico, University of Lisboa, Av. Rovisco Pais, 1049-001 Lisbon, Portugal
[d] Centro de Química de Coimbra - Institute of Molecular Sciences (CQC-IMS), Departamento de Química, Faculdade de Ciências e Tecnologia, University of Coimbra, 3004-535 Coimbra, Portugal
[e] Faculty Pharmacy, University of Coimbra, Pólo das Ciências da Saúde, Azinhaga de Santa Comba, 3000-548 Coimbra, Portugal
[f] Department of Medical Oncology, Cancer Center Amsterdam, Amsterdam University Medical Centers (Amsterdam UMC), Vrije Universiteit Amsterdam, The Netherlands
[g] Cancer Pharmacology Lab, Fondazione Pisana per la Scienza, Pisa, Italy
[h] Department of Engineering and Chemical Sciences, Karlstad University, 65188 Karlstad, Sweden

ARTICLE INFO

Keywords:
Isatin
Necroptosis
Live cell imaging
Non-small cell lung cancer

ABSTRACT

Isatin derivatives have attracted a lot of interest for their potential in the development of new anticancer drugs. A library of 38 isatin derivatives, created through an Ugi four-component reaction, underwent an initial screening in a panel of six human solid tumor cell lines. The four most active derivatives were then selected for further testing. These compounds showed selectivity towards the non-small cell lung cancer (NSCLC) cell line SW1573, whilst NSCLC A549 cells were barely affected. The combination of phenotypic assays, including wound healing, clonogenic and continuous live cell imaging provided a deeper understanding of the compounds' mode of action. In particular, the latter demonstrated that isatin derivatives were able to induce necroptosis in SW1573 cells. The kinetics of cell death showed that necroptosis appeared after 2.5 h of exposure, which could be delayed to 7 h when co-treated with necrostatin-1. Interaction between the isatin derivatives and the KRAS G12C protein variant was discarded after in silico studies. Further studies are warranted to identify the cellular target responsible for the observed selectivity among cell lines.

1. Introduction

Isatin (1*H*-indole-2,3-dione, Fig. 1) is a natural compound first isolated from the fruits of *Couroupita guianensis*, but it is found in other plants worldwide, including *Isatis tinctoria*, *Melochia tomentosa*, and *Boronia koniamboensis* [1]. In humans, isatin is produced as a metabolite of tryptophan or epinephrine (adrenaline). Endogenous isatin inhibits monoamine oxidase (MAO), with preferential binding to MAO-B isoform [2]. Chemically, isatin can be synthesized in a straightforward manner, which has encouraged medicinal chemists to prepare a myriad of derivatives in the search for novel compounds with pharmacological applications. Several isatin-based molecules behave as tyrosine kinase receptor inhibitors (iRTK). The kinase targeting effect is mainly produced due to the indolic nature of these molecules, which resembles the natural substrate of kinases (i.e. ATP). In fact, several studies showed preclinical evidence of antiproliferative activity of isatin derivatives through the interaction with other kinases. Thus, isatin derivatives exhibit anticancer, antitubercular, antimalarial, antifungal, antibacterial, anticonvulsant, and antiviral properties, among others [3,4]. In the field of cancer therapy, there has been a substantial amount of research dedicated to the study of isatin derivatives [5]. As a result of these efforts, isatin derivatives (Fig. 1) sunitinib and toceranib are currently approved for the treatment of various cancer types, whereas semaxanib, orantinib, nintedanib, and esperidin are undergoing clinical trials [6].

Recently, we explored the antiproliferative activity of a small library of 38 isatin derivatives prepared by an Ugi four-component reaction [7]. The biological screening against a panel of six human solid tumor cell lines (A549, HBL-100, HeLa, SH-SY5Y, T-47D and WiDr) revealed that the majority of the compounds display antiproliferative activity in the

* Corresponding author.
E-mail address: jmpadron@ull.es (J.M. Padrón).

https://doi.org/10.1016/j.bcp.2024.116059
Received 3 November 2023; Received in revised form 12 February 2024; Accepted 13 February 2024
Available online 15 February 2024

List of abbreviations

ATCC	American type culture collection
ATP	Adenosine triphosphate
EHT	Extended Hückel Theory
FCS	Fetal calf serum
GI_{50}	50 % growth inhibition
iRTK	Tyrosine kinase receptor inhibitors
MAO	Monoamine oxidase
MOE	Molecular Operating Environment
NSCLC	Non-small cell lung cancer
PBS	Phosphate buffer saline
PCR	Polymerase chain reaction
PDB	Protein data bank
SAR	Structure-activity relationship

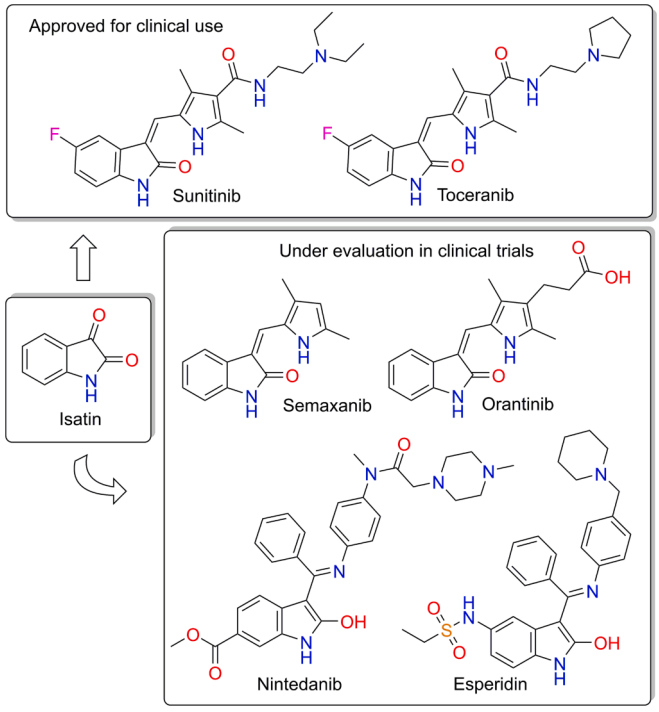

Fig. 1. Chemical structure of isatin and its clinically relevant anticancer derivatives.

low and sub-micromolar range. Analysis of the GI_{50} values provided information on the structural requirements involved in tumor cell growth inhibition. From this initial test, a subset of four compounds (**1**–**4**, Fig. 2) was selected for further mechanistic studies. The structure–activity relationship (SAR) study revealed that critical factors for activity were the presence of a halomethylene group and the functionalization on the benzene ring with halogen (**1** and **3**) or alkyl (**2**) groups.

During the course of those investigations, we found very strong growth inhibition at the nanomolar range against the non-small cell lung cancer (NSCLC) cell line SW1573. This was an unexpected result considering that the GI_{50} values for such compounds against the NSCLC cell line A549 were in the range 1.0–2.2 μM [7]. Therefore, we turned our attention to get a deeper understanding of the sensitivity of SW1573 cells to this particular family of compounds. Indeed, it was observed that sensitivity to the Ugi products varied strongly between cell lines. This variability provides an opportunity to identify compounds with specific selectivity towards a particular phenotypic feature of a tumor.

In this work, we describe the extensive molecular pharmacological profiling carried out on a subset of the isatin derivatives (**1**–**4**) that led to the identification of necroptosis as the mode of selective cell killing in specific NSCLC cells.

2. Materials and methods

2.1. Isatin derivatives

The synthesis and characterization of isatin derivatives **1**–**4** was reported earlier [7].

2.2. Cell lines

The human solid tumor cell lines used in this study were the non-small cell lung cancer SW1573, A549, H23, the pancreatic cancer MIA PaCa-2, and the colon cancer LS174T. Cell lines were obtained from the American Type Culture Collection (ATCC, Manassas, VA). The cell lines were tested for their authentication by PCR profiling using short tandem repeats, which was performed by BaseClear (Leiden, The Netherlands). The maintenance of cell cultures was in 60 mm Petri dishes in a humidified air incubator (37 °C, 5 % CO_2, 95 % humidity). The cell culture medium used was RPMI 1640 supplemented with 5 % heat inactivated FCS, 2 mM L-glutamine, 100 U/mL penicillin and 0.1 mg/mL streptomycin. Cell cultures were passaged biweekly using 0.05 % trypsin and maintained at low passage. Single cell suspensions were counted using Moxi Z automated cell counter.

2.3. Cell migration studies

To obtain confluent monolayers of A549 cells onto 24-well plates, the cell seeding density was 10,000 cells per well. A wound was made using a sterile scratch tool to each well. Next, cells were washed with PBS to remove the debris produced by the manipulation. Then, new medium with or without compounds **1**–**4** was added. Two doses were selected, a low (equivalent to the GI_{50}) and a high dose (5X GI_{50}).

The wound closure was monitored by phase-contrast microscopy and photographed at the start of the experiment (t_0) and after 6 h of exposure

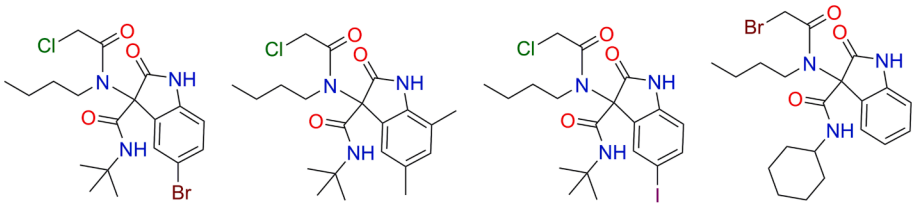

GI_{50} = 0.0063–1.2 | GI_{50} = 0.023–1.0 | GI_{50} = 0.000097–1.4 | GI_{50} = 0.029–2.2

Fig. 2. Structure of isatin derivatives **1**–**4** and their antiproliferative potency (GI_{50} range, μM) against the human solid tumor cell lines A549, HBL-100, HeLa, SH-SY5Y, T-47D and WiDr [7].

(t_6). Pictures of the plates were taken using the Universal Grab 6.3 software (DCILabs) from a computer connected to a Leica microscope with a JAI TMC-1327 camera.

The percentage of migration was calculated using the following equation:

% Migration = 100 x (Wound area at t_0 – Wound area at t_6) / (Wound area at t_0).

2.4. Clonogenic assay

SW1573 cells were seeded onto 6 well plates at a density of 450 cells/well and allowed to attach to the well surface. Then, two doses of the selected isatin derivatives were added (10 and 50 nM) to the respective wells. After 30 min of exposure, the growth medium was replaced with drug-free medium and the cells were placed in the incubator for 7 days, checking every day the level of humidity. Cells were fixed with methanol and stained using crystal violet (0.5 % w/v in deionized water), removing the excess rinsing carefully with water. Colonies were counted using AutoCellSeg, a free software implemented in MatLab that allows automatic segmentation of the colonies [8].

2.5. In silico studies

Interactions of KRAS with the isatin derivatives **1**–**3** were analyzed by computational docking using Molecular Operating Environment (MOE) software (Chemical Computing Group ULC, Montreal, Canada). The crystallographic three-dimensional structure of the human KRAS G12C covalently bound to AMG 510 was obtained from PDB (6OIM). The protein was prepared using Amber10 force field with EHT parameters, R-field solvation model, dielectric constant of 1 for the protein inside and 80 for outside. Ligand structures were drawn in MOE software, and their energies were minimized using Amber10 force field with EHT parameters for small molecules, using as stop criterion an RMS gradient lower than 0.01 kcal/mol/Å. For the docking calculation, since catalytic waters participate in the intrinsic hydrolysis of GTP and support a simultaneous triple proton step, only those molecules dictating more than 5 Å from the ligand were eliminated. Covalent docking was performed using the Covalent Docking tool in MOE selecting Michael Addition. The grid was defined around the refined structure by centering on the crystallized ligand, Cys12 was set as the reactive residue and the reaction. Triangle Matcher algorithm with the London dG scoring scheme was employed. In the refinement stage we kept the receptor rigid and used the GBVI/WSA dG scoring scheme.

2.6. Label-free continuous live cell imaging

A549 and SW1573 cells were seeded onto 35 mm high glass-bottom μ-dish (IBIDI, Germany) at a density of 80,000 cells/dish. After 24 h, growth medium was replaced for RPMI 1640 phenol red-free medium and cells were treated with 100 nM of the selected isatins for 15 h, Using the CX-A label-free cell imaging system (Nanolive S.A., Switzerland) the status of the cell population was recorded every 5 min. The initial field of observation was selected considering a homogeneous distribution of cells, and the field view was 236 μm x 236 μm. After acquisition, images were processed using Eve segmentation and analysis software (Nanolive S.A., Switzerland) to evaluate cell content and morphology parameters (Eve Analytics) as well as the mode of cell death induced (Live Cell Death Assay, LCDA). The measurements were obtained for each individual in the population at each time point for every treatment.

2.7. Fluorescence labelling in continuous live cell imaging

Bis-Benzimide H33342 trihydrochloride (Hoechst 33342) was used to stain nuclear compartments in live cells. Cells were seeded as previously described in section 2.6 and Hoechst 33342 staining was performed before the treatment was added. Briefly, 1:2000 dilution in RPMI was performed from a stock of 10 mg/mL (deionized water). Cells were incubated for 10 min in dark conditions, medium was removed and cells washed once with PBS with Ca^{2+} and Mg^{2+}. Whilst label-free imaging was performed following aforementioned conditions, fluorescence signal was recorded every 20 cycles using the DAPI-UV filter. Time of exposure and signal amplification were selected empirically before recording.

2.8. DAPI staining

A549 and SW1573 cells were seeded onto 6-well plates containing sterile coverslips at the bottom in a density of 100,000 cells/well. After 24 h, compounds were added at 50 nM and incubated for 18 h. Cells were fixed with 4 % PFA (PBS) for 10 min at RT and then washed in 50 mM NH_4Cl for 10 min to reduce PFA background. After rinsed with PBS, 0.1 % Triton solution was added during 10 min to permeabilize cells to DAPI and subsequently rinsed with PBS. Staining was performed using DAPI solution (1 μg/mL in methanol) for 10 min in absence of light. After rinsing with PBS, coverslips were mounted on a microscopy slide over a drop of mowiol mounting medium and sealed using nail polish to avoid loss of volume. Random fields of observation were imaged using 20X and 40X magnifiers in a LEICA DM 4000B microscope (Leica Microsystems) with the A excitation filter (BP 340/380 nm).

2.9. Propidium iodide staining

Necrosis was evaluated using propidium iodide (PI) staining. SW1573 cells were seeded onto a 96 well dark-wall clear-bottom plates at a density of 10,000 cells/well and incubated for 24 h. Then, cells were exposed to two concentrations (50 and 100 nM) of the isatin derivatives. After 4 h, medium was removed carefully and cells were incubated with PI solution (5 μg/mL in PBS) for 10 min in dark conditions. Fluorescence signal of PI was measured using Varioskan Lux Multimode plate reader at 538/617 nm excitation/emission wavelength.

2.10. Statistics

Data are presented as mean values ± standard deviation in at least three independent experiments. Statistical analysis was performed through Microsoft Excel, using two-tailed Student's *t*-test to generate *p* values. Significance was considered when $p < 0.05$.

3. Results

3.1. Effects on cell migration

Chemical compounds based on an isatin scaffold behave as modulators of the migratory activity in cancer cells, reducing their motility through their interaction with MMP-2 and MMP-9 [9,10]. In order to investigate if isatins **1**–**4** were able to modify cell migration, we conducted a wound healing assay. Accordingly, A549 was the cell line selected for this test due to its migration rate. Moreover, its ability to form a homogenous confluent monolayer enables us to study the unidirectional movement of the cells, becoming an exceptional model for this kind of assay [11].

The test revealed that all the compounds were able to reduce the ability of the wound to close after 6 h of exposure when using a dose five times its GI_{50} (5X GI_{50}) (Fig. 3). In the case of the selected isatins, their high potency limited the exposure time to 6 h in order to avoid cytotoxic effects during the assay. If the compounds induce cell death, the wound generated will remain open, creating a false positive outcome. The halogen-phenyl isatins **1** and **3** showed the best results in terms of reduction of cell migration, diminishing the wound closure in 39 % and 38 %, respectively. Untreated cells (control) were able to close the discontinuity by 61 %. Isatins **2** and **4** also reduced the migration of cells in a significant manner although at a lower level (49 % and 46 %,

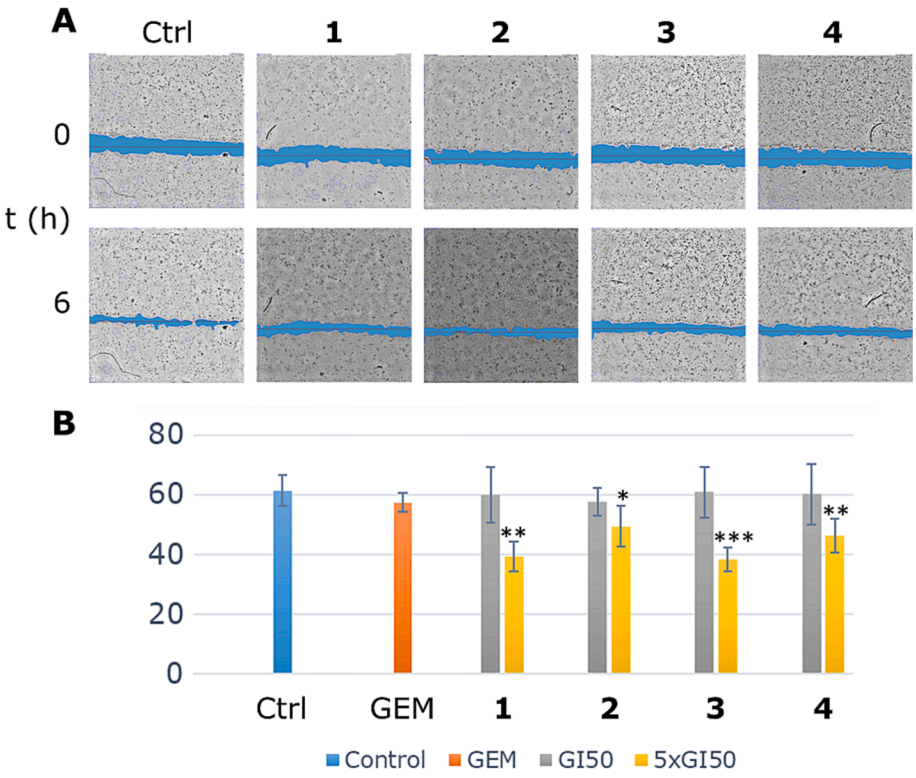

Fig. 3. **A**: Representative images of the wound closure assay after 6 h of exposure. A549 cells were exposed to isatins **1**–**4** at two doses, GI_{50} and 5X GI_{50}. Gemcitabine (GEM) at 5X GI_{50} was used as reference. **B**: Percentage of wound closure compared to untreated control. Wound area was measured at 0 and 6 h. Error bars: SD after at least three independent experiments. *$p < 0.05$; **$p < 0.01$; ***$p < 0.001$ vs. untreated cells (Ctrl).

respectively). The antimigratory activity was dependent on drug concentration since the effect is barely produced when cells were exposed to the GI_{50} dose. These results are in line with previous studies in other cell models with halogenated isatin derivatives at similar concentration range [12].

3.2. Effects on cell lines with diverse KRAS status

One of the differences reported in the literature between A549 and SW1573 cell lines is their KRAS status. Although this was not the main goal of this study, we wondered if the observed differences in sensitivity related to KRAS status could provide some hints for further investigating the mode of action (MoA) of the compounds. A549 presents a missense mutation at codon 12 of the oncogene that substitutes a glycine for a serine (G12S) [13], whilst SW1573 harbors a missense substitution of a glycine for a cysteine (G12C) [14]. In our cell bank, another two KRAS G12C cell lines were available. NSCLC cell line H23 was included in the pool of assays. This cell line, besides the KRAS G12C mutation, also harbors an endogenous missense mutation –M246I– in p53 that alters it function and fails to induce apoptosis [15]. The KRAS G12C PDAC cell line MIA PaCa-2 was also selected [16]. Finally, the panel was completed with the colon cancer cell line LS174T, which is reported to have the KRAS mutation G12D [17]. Table 1 shows the effects on cell growth (expressed as GI_{50}) after 48 h of exposure. Overall, the four compounds were markedly less active against A549 and LS174T cells, with GI_{50} values in the range of 1.0–2.2 μM. In H23 cells, the most potent compound was **3** displaying a GI_{50} value below 100 nM. Notably, the compounds were more active against the G12C cell lines, with GI_{50} values in the low nanomolar range. Derivatives **1** and **3** exert an antiproliferative activity in the same order of magnitude in SW1573 and MIA PaCa-2 cells with a slight loss of potency for compound **2.** Hence, the KRAS status seemed relevant, although not sufficient to explain the potency of the isatin derivatives. At this point, isatin **4** was discarded from further assays. This decision was consistent with the existing SAR highlighting the relevance of the halomethylene group while extending the SAR to the functionalization on the benzene ring with halogens (Br in isatin **1**, and I in isatin **3**).

Table 1
Antiproliferative activity (GI_{50}, nM) of isatins **1**–**4** against cell lines with diverse KRAS status.

	Isatin derivative			
Cell line	**1**	**2**	**3**	**4**
A549	1311 ± 261	1004 ± 378	1038 ± 192	2185 ± 315
H23	299 ± 36	174 ± 67	17 ± 4.3	160 ± 62
SW1573	2.3 ± 0.2	3.3 ± 1.2	2.0 ± 0.4	14 ± 6.3
MIA PaCa-2	3.8 ± 1.3	13 ± 2.6	1.9 ± 0.6	24 ± 3.1
LS174T	1793 ± 139	1751 ± 198	1567 ± 285	15807 ± 4154

Values represent mean ± standard deviation of at least three independent experiments.

3.3. In silico studies

Encouraged by the previous results, we decided to run in silico experiments to check for a hypothetical interaction between the drug candidates **1**–**3** and protein KRAS G12C. In the catalytic activity mechanism of KRAS, water molecules participate directly in the conversion of GTP to GDP. During the hydrolysis, a molecule of water acts as a nucleophile whilst another molecule adopts an assistant role for a proton transference. When the GTP is bound to Tyr32, the nucleophilic attack on the γ-phosphate of the nucleotide leads to a proton shuffle, released by the catalytic water. The assistant nucleophilic water molecule is activated by Gln61, protonates the oxygen of γ-phosphate, forming the resultant GDP and $H_2PO_4^-$ [18]. More importantly, when the G12C mutation is present, the side chain of the substituent Cys displaces

Gln61, inducing extra exposure of the binding pocket toward the solvent (cytoplasm). Through this change, catalytic water molecules get destabilized and the GTP hydrolysis is slightly affected negatively [19]. Because of this, water molecules surrounding the active site –at a distance of less than 5 Å– were kept during the simulations.

For the in silico studies, the crystal structure of the KRAS G12C variant bound to the approved drug sotorasib was obtained from PDB (6OIM). The mechanism of interaction between the protein and the potential ligands was set previously based on the crystal ligand used as a model. Sotorasib directly interacts with KRAS G12C in its inactive state, forming a covalent bond with the mutated Cys12 through the acrylamide group [20]. The ability of sotorasib to bind to the inactive state of KRAS is possible because of the G12C mutation present. In contrast, the other mutant variants in the presence of sotorasib keep the GTPase activity of KRAS similar to the wild type [21]. Hence, sotorasib is ineffective against other KRAS isoforms as noted previously. Adagrasib –another drug approved for clinical use– forms the same crucial covalent bond through an acrylamide moiety with C12 of the mutated KRAS [22]. Similarly, several KRAS G12C targeting compounds validated in preclinical models have shown this covalent union [23].

Considering this, it was concluded that a Michael addition should be the preferred type of covalent binding reaction to take place. This approach was validated through the calculation of the binding energy of the co-crystallized ligand, resulting in good RMSD and docking score values. However, none of the isatin derived compounds **1**–**3** were suitable for this type of interaction with the protein due to structural requirements. Michael addition needs the presence of α,β-unsaturated carbonyl to take place, a functional group not present in the isatin library evaluated. By contrast, due to the presence of halogens in the selected isatins, a nucleophilic substitution was selected as the type of reaction to simulate. Although a few compounds from the library were docked, none of the selected ones was suitable for this type of reaction. In light of these results, a direct interaction with KRAS G12C following this binding approach was discarded. Thus, we moved our attention to evaluate the differential response of A549 and SW1573 cells toward isatins **1**–**3**.

3.4. Effects on reproductive viability

The clonogenic assay is a versatile and frequently used tool to quantify reproductive cell survival in vitro. To assess this effect clonogenic assays were performed in the most sensitive cell line, i.e. SW1573. The results are shown in Fig. 4. Two doses were selected –low 10 nM, high 50 nM– to assess dose dependency. The exposure time to isatin derivatives (**1**–**3**) was set to 30 min, after which time, cells were refreshed with drug-free medium. After 8 days of incubation, wells exposed to the high dose did not show formation of cell aggregates whilst a considerable number of colonies were observed in untreated controls. Treatment with a lower dose also reduced the number of colonies although not so drastically. Interestingly, differences were observed between the compounds. Isatins **1** and **3** were able to reduce the number of colonies with statistical significance, especially **1**, whilst **2** only produce a slight decrease. These results demonstrate that a short exposure time to the compounds is enough to produce a significant effect even if the drugs are removed from the medium. With only 30 min of incubation, the effect observed suggest that the compound absorption is rapid and that either the effects exerted by the compounds in such a short period of time are sufficient to produce the antiproliferative effect or that the drug is maintained inside the cells even when the medium is replaced. This test also pointed out that the functionalization on the benzene ring with halogen (**1** and **3**) gave the best results.

3.5. Getting insight on the mode of cell death

Continuous live cell imaging allows to analyze the potency of the compounds and their predominant mode of death, in addition to the kinetics of cell death. In this test, A549 (Supplementary Video S1) and SW1573 (Supplementary Video S2) cells were exposed to 100 nM of the selected isatins for 20 h, recording at intervals of 5 min. In A549 cells, compounds **2** and **3** induced notorious cell death after 15 h of exposure with less than 20 % and 40 % of the population affected, respectively (Fig. 5A), whilst isatin **1** did not induce cell killing. When the same conditions were applied to SW1573 cells, all the population was dead before 5 h of exposure (Fig. 5B). The predominant death phenotype resembled necrosis, with cells increasing their volume drastically, showing circled nucleus and loss of plasma membrane.

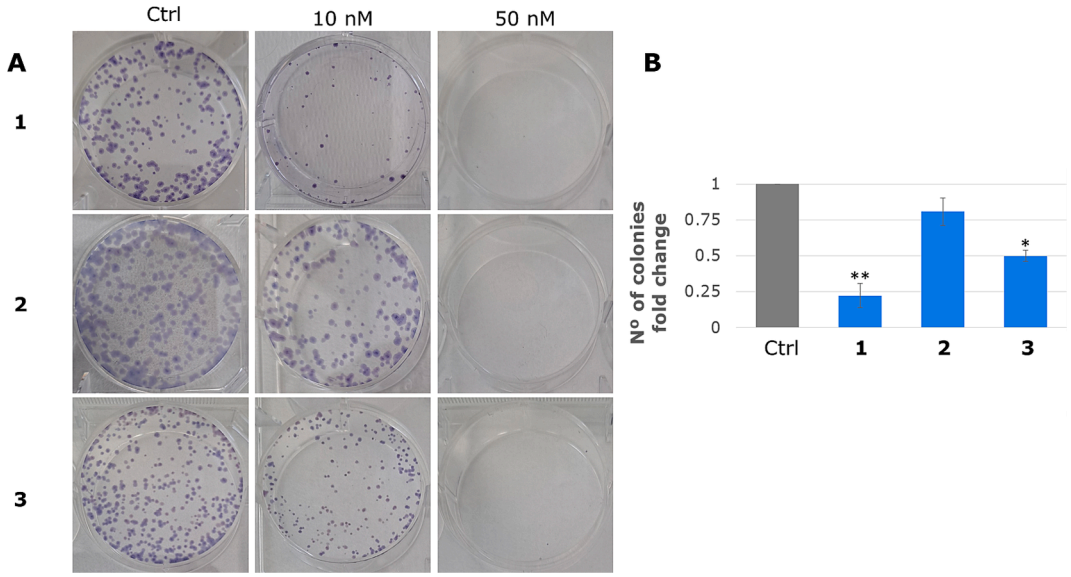

Fig. 4. Clonogenic assay performed on SW1573. Cells were exposed to two different doses of the compounds for 30 min and placed in the incubator for 8 days. **A**: Representatives images of the colony formation under each treatment. **B**: Average number of colonies growth in the samples treated with 10 nM of each compound expressed as relative to the number of colonies in the untreated samples. Error bars: SD after 3 independent experiments. *p < 0.05; **p < 0.01 vs untreated cells (control).

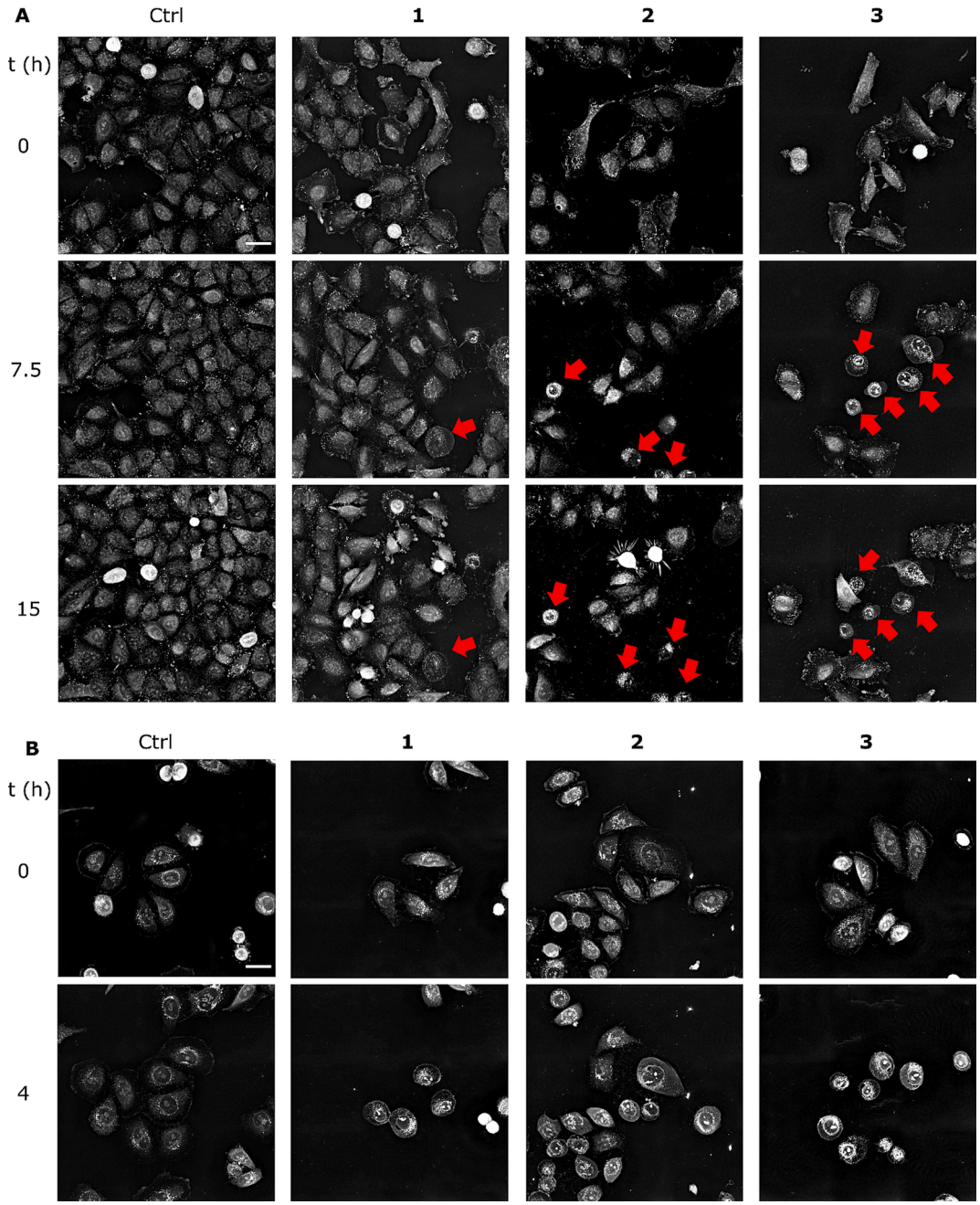

Fig. 5. Representative snapshots of A549 (A) and SW1573 (B) cells exposed to 100 nM of the selected isatins **1**–**3** for 15 h. Red arrows indicate the presence of cells undergoing necrotic death. Scale bar 30 μm.

After the segmentation analysis, the LCDA allowed to study the kinetics of cell death in A549 and SW1573 cells (Fig. 6). In all cases, cell death occurred via necrosis. However, the kinetics and the affected cell population was different between cell lines and treatments. Thus, necrosis in A549 cells started around 4 h after exposure to **2** and **3**. Noteworthy, **1** did not induce cell death in A549 cells (Fig. 6A-B). In contrast, SW1573 cells were very sensitive to all the isatin derivatives. Necrosis started almost at the onset of the exposure and affected nearly 100 % of the cell population (Fig. 6C-D). The induction of cell death in such an extensive way at short times of exposure indicates that the modifications produced in cells do not require prolonged incubation with the compounds. This observation is consistent with the results obtained with the clonogenic assay (Fig. 4).

Furthermore, necrosis was supported by the metrics provided by the system after segmentation analysis (Fig. 7). Thus, treated cells showed an overall reduction of cell area compared to untreated control. This effect was particularly notorious for **2** and **3** at the onset of incubation and being stable for the rest of the observation period (Fig. 7A). This reflects the speed of the morphological effects produced, which started with cell swelling but rapidly produced diminishing of cell area due to cell death. Concomitantly, the drastic decrease of dry mass in treated cells as opposed to the untreated samples that exhibited minimal changes over time, indicates the release of cell content to the extracellular medium due to the disruption of the cell membrane, a characteristic feature of necrotic cell death (Fig. 7B).

Shape, form factor and compactness are parameters that quantify the loss of cell polarity under treatment. Form factor measures the circularity of the segmented object, representing a perfect circle with a value of 1 (Fig. 7C), and depicts how all three treatments induced an increase in form factor as a consequence of cell swelling and rounding. The

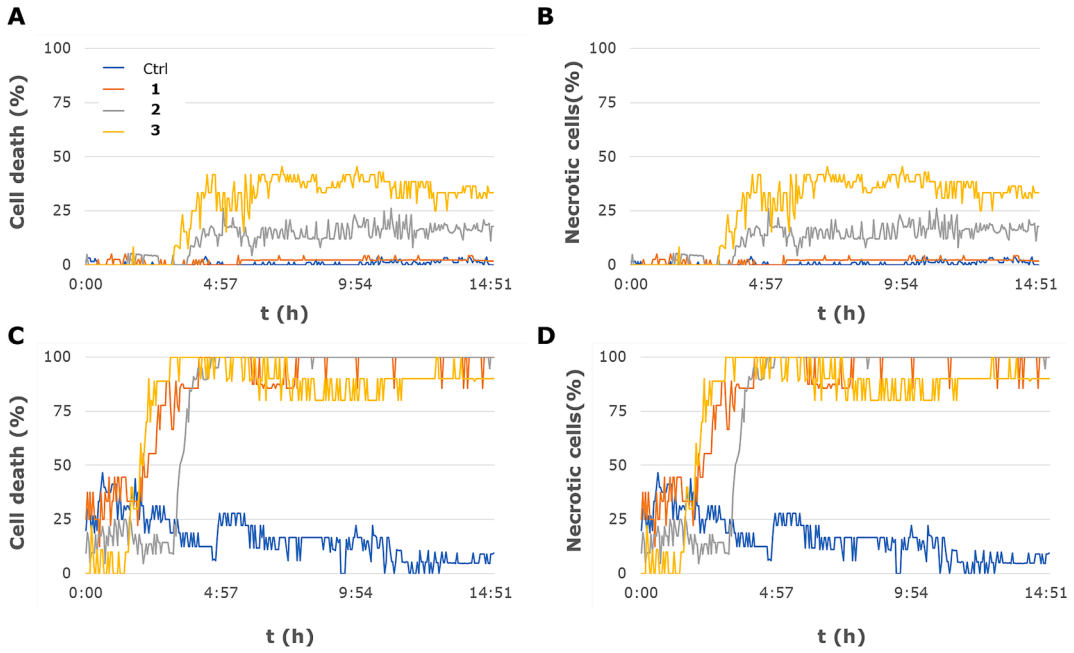

Fig. 6. Kinetics of cell death and number of necrotic cells (%) in A549 (A-B) and SW1573 (C-D) cells treated with isatins **1**–**3** at 100 nM for 15 h. Cells were monitored every 5 min. At each time point, the segmentation analysis provided the death and necrotic percentage of dead cells within the population.

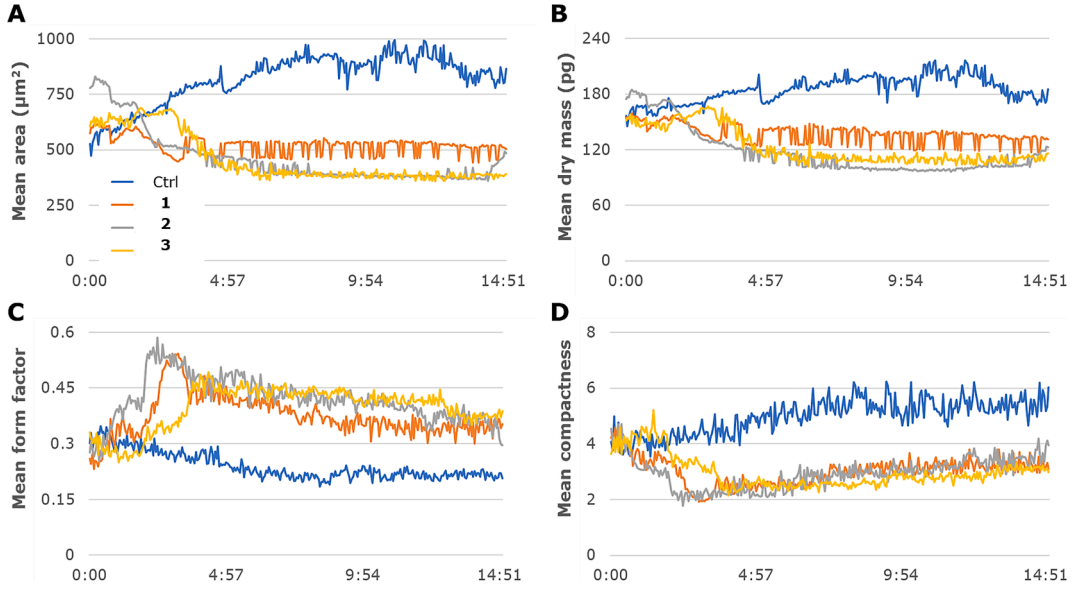

Fig. 7. Kinetics of morphological and cell content parameters of SW1573 cells untreated or treated with isatins **1**–**3** over 15 h of exposure. Cells were monitored every 5 min. At each time point, the segmentation analysis provided morphological and cell content parameters.

subsequent decrease occurred due to the loss of cell structure during necrosis progression, whilst the control group remained within the same range due to the maintenance of the cell shape. A similar effect was observed in the evolution of compactness, which estimates a filled circle with a value of 1 and considers irregular objects or those containing holes with values > 1. Higher values were observed in cells without treatment due to the epithelial morphology of SW1573 cells (Fig. 7D). The decrease observed during the first hours of exposure to the isatins **1**–**3** could be attributed to the previously mentioned necrotic cell rounding, as well as the slight increase response to the cell content leakage.

3.6. Isatin derivatives induce necrosis in SW1573 cells

Necrosis can be triggered by several factors, among which irreparable DNA damage stands out. To study DNA damage, DAPI staining was performed for a better observation of the nuclear affection (Fig. 8). After 24 h of exposure to 50 nM of isatins **1**–**3**, SW1573 cells showed a noticeable reduction in the area of the nucleus, along with fragmented nuclear material (Fig. 8B). Apoptotic phenotypes tend to increase DAPI fluorescence signal due to the nuclear condensation that precedes cell shrinkage [24]. However, the microscopical observations of isatin-treated SW1573 cells suggested loss of nuclear material since the stained objects were less compact and the fluorescence was markedly diminished. Measurement of the pixel intensity of each cell

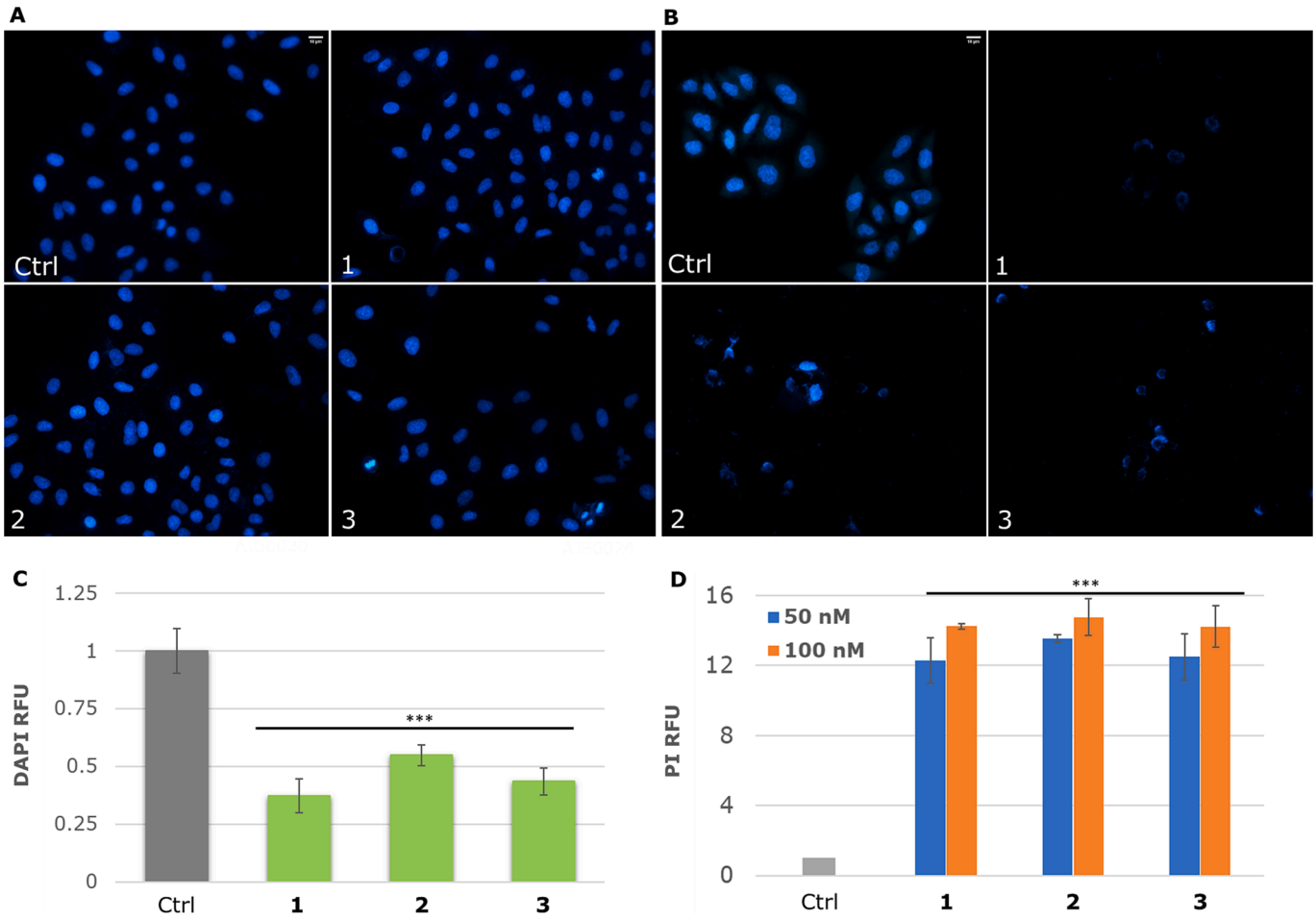

Fig. 8. Study of the nuclear modifications through fluorescence staining. Representative images of A549 (**A**) and SW1573 (**B**) cells stained with DAPI after 24 h of exposure to 50 nM isatins **1**–**3**. Scale bar 10 μm **C**: From the set of images of isatin-treated SW1573 cells, a quantification of the fluorescence signal of every single cell was performed and plotted as relative fluorescence units compared to control. **D**: Relative fluorescence units of PI staining of SW1573 cells after exposure to isatins **1**–**3** for 4 h. Error bars represent standard deviation from at least three independent experiments. *** $p < 0.001$ vs control.

demonstrated that the DAPI signal was decreased (Fig. 8C), a characteristic of DNA content reduction. These could suggest that DNA damage and nuclear leakage could have taken place due to the action of the compounds. On the other hand, A549 cells treated equally did not show remarkable effects on nuclear alteration.

Thereupon, necrosis was evaluated in SW1573 cells through PI uptake. In a healthy situation, PI is unable to penetrate in the cells. When necrosis occurs, cell membrane is disrupted, allowing this fluorescent

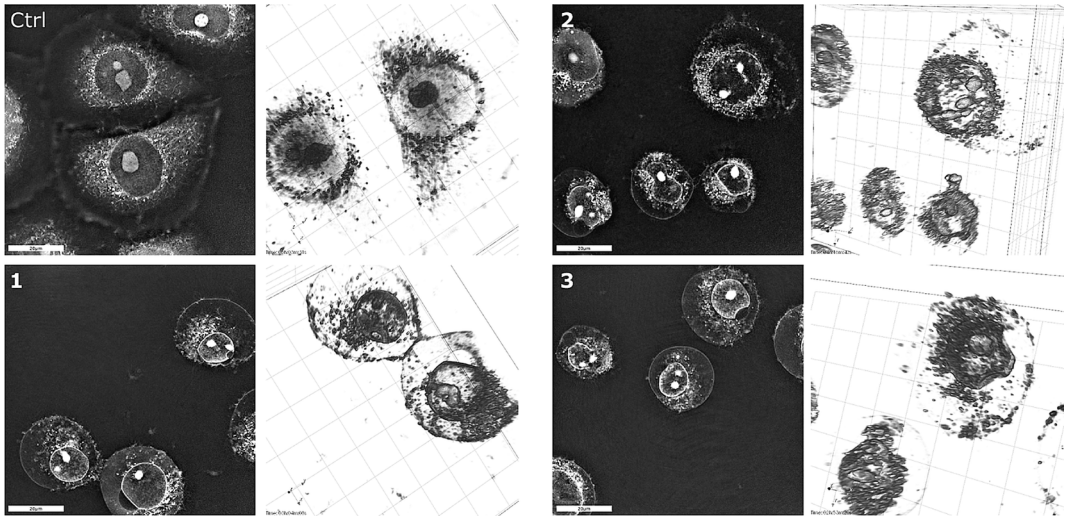

Fig. 9. Representative images of untreated SW1573 cells (control) or exposed to 100 nM of the indicated compounds. For every condition left images represent the effect after 5 h of exposure. Right images are the corresponding 3D holotomographic reconstructions of selected cells from these samples. Scale bar 20 μm.

dye to enter in the intracellular space. Then, PI intercalates in double stranded DNA, producing a metachromatic shift from 493/636 nm to 535/617 nm and increasing the quantum yield [25]. PI fluorescence was measured in a microplate reader in cells exposed to 50 and 100 nM of each three compounds for 4 h. Fluorescence signal was highly increased compared to untreated cells exposed to the same procedure, supporting the morphological changes observed in the live cell experiments (Fig. 8D). When comparing the two doses used it was observed that the increase in fluorescence in the 100 nM samples was modestly higher than when using the 50 nM dose. This is consonance with broad necrotic phenotypes observed in other experiments, which shows a slight dependence on the concentration of the isatin derivatives applied at this nanomolar range.

Holotomographic imaging allowed a three-dimensional (3D) representation of the cellular entities, facilitating the observation of structural alterations. This technique confirmed the previously noted cell swelling and the loss of cell content after treatment with the isatin derivatives (Fig. 9). After 5 h of exposure, SW1573 cells presented an inflated morphology, with rounded nucleus and clear loss of density. Whilst the nucleus structure was preserved and the nucleolus is still observed in the untreated samples, treated cells showed clear disruption of the nuclear morphology and less compacted nucleolus. Moreover, limits of the nuclear envelope were barely detected in the 3D images, similarly to the absence of cellular membrane. This pattern also matched the leakage of cellular components to the extracellular environment, the aforementioned characteristic phenotype of necrotic cell death that was also detected by the augmented amount of cell debris in the live-cell microscopy assays [26].

Next, we moved to observe the kinetics of nuclear changes in SW1573 cells using live imaging (Supplementary Videos S3). Hoechst 33342 staining showed the similar results obtained with DAPI, i.e. loss of signal due to the DNA degradation and extended nuclear affectation (Fig. 10). The cell swelling was observed in the perinuclear space, while the nucleus experimented rounding of their shape and a clear size reduction after only 3 h of exposure. Interestingly, although the fluorescent signal decreased toward the end of the treatment, an increase in the intensity was observed around 6 h of treatment. However, no evidence of apoptotic bodies was observed prior to death. Subtle differences were observed between the three isatin compounds, especially regarding the time necessary to observe the effects, but the mode of cell death was highly common overall. Taking all together, these results indicate that necrosis might be the mode of cell death induced by the isatin derivatives **1**–**3**, and the loss of signal observed through endpoint experiments is a process that evolves during time.

3.7. Isatin derivatives induce necroptosis in SW1573 cells

Necrotic cell death has been commonly related to uncontrolled events and mostly triggered by non-specific harsh stimuli. However, many experimental evidences have shown how some forms of necrotic cell death can occur in a tightly regulated way [27]. Necroptosis is one of these modes of regulated necrotic cell death that presents phenotypic characteristics identical to uncontrolled necrosis, such as cell swelling or membrane disruption [28]. In order to evaluate if the isatin derivatives were inducing necroptosis, SW1573 cells were pre-incubated with 40 μM of necrostatin-1 (Nec-1) –a known inhibitor of necroptosis [29]– for 30 min and the isatins **1**–**3** were subsequently added. The effects were observed using live cell microscopy (Supplementary Videos S4). As depicted in Fig. 11, necrostatin-1 was able to prevent the occurrence of cell death with complete absence of any individual with the morphological features observed during the treatment with the isatin derivatives alone for at least 7 h, whilst in the absence of necrostatin-1 single cells with these features appeared before 2.5 h. If the induction of an extended effect on the population is studied the differences become

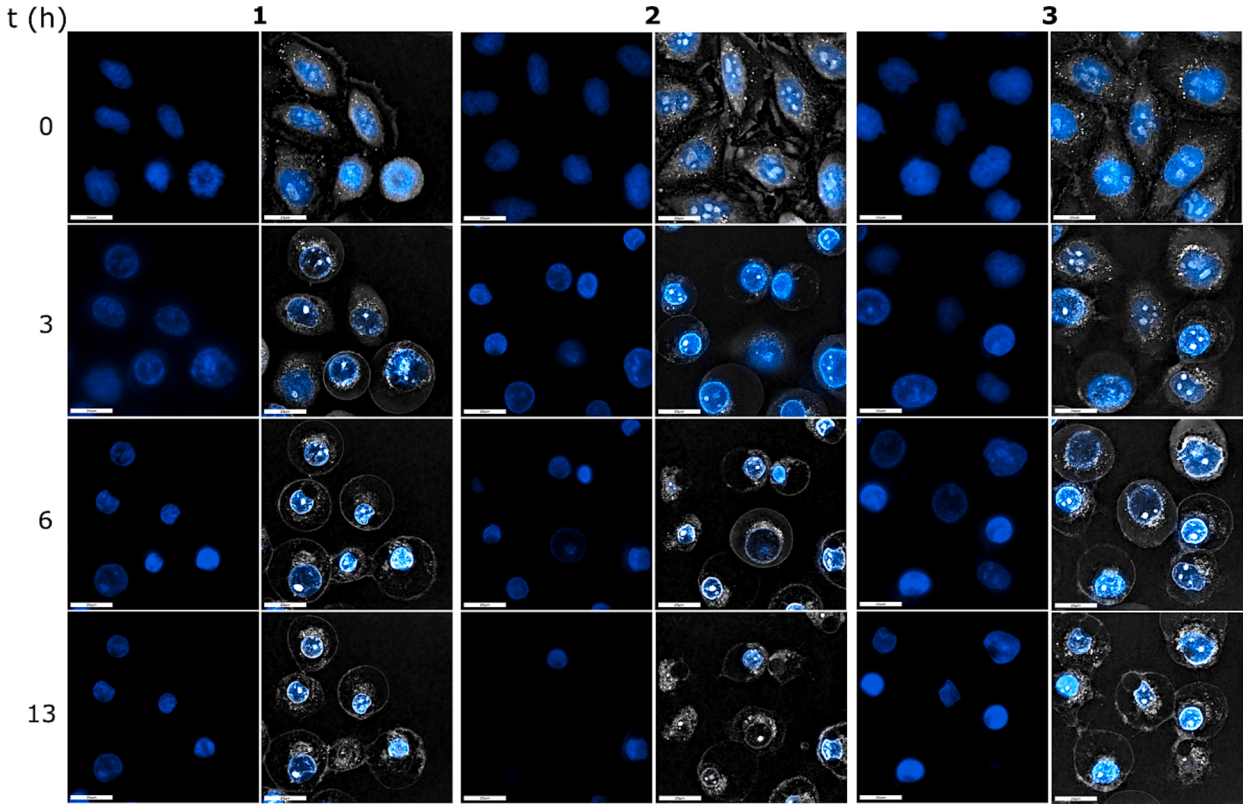

Fig. 10. Representative images of live imaging acquisition at different time intervals of SW1573 cells treated with 100 nM of isatin derivatives **1**–**3** for 15 h and stained with Hoechst 33342. Left panels represent Hoechst fluorescence channel only, right panels are merged images with refractive index acquisitions. Scale bar 20 μm.

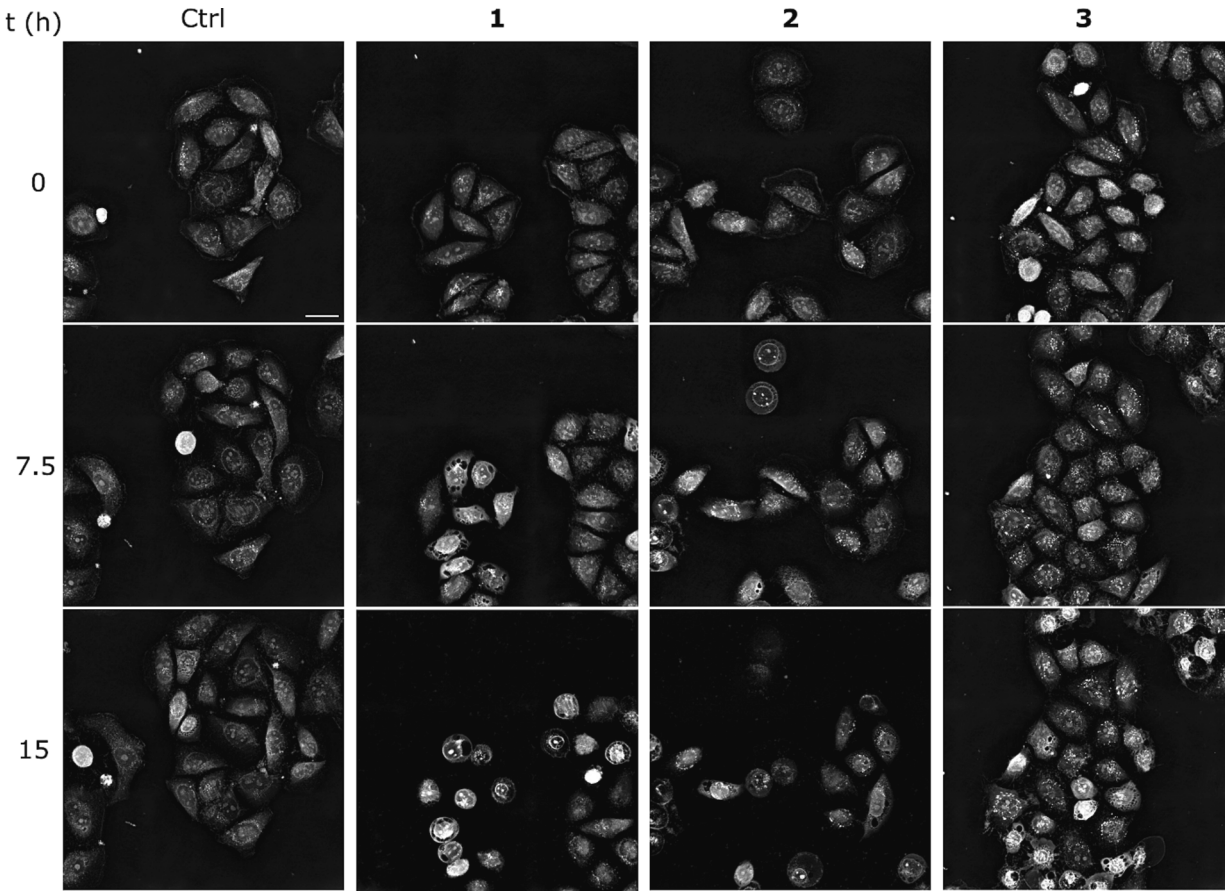

Fig. 11. Representative snapshots at different time intervals of SW1573 cells treated with Nec-1 at 40 μM either alone or in combination with 100 nM of isatins **1**–**3** for 20 h. Scale bar 30 μM.

even more pronounced. As shown before, the isatin derivatives were able to produce total cell death in the population after 4 h of exposure (Fig. 5B). Pre-incubation with the necroptosis inhibitor delayed the extended cell death until more than 15 h of treatment. Noteworthy, necroptotic cell death morphologies in both treatments (alone and in combination with Nec-1) were observed eventually, probably due to the high concentration of isatin derivatives used in the assays when compared to their GI_{50}.

After segmentation analysis, we found substantial differences when comparing the treatments with or without the co-incubation with Nec-1 (Fig. 12). First, mean cell area of the population did not decrease when SW1573 cells were co-incubated with Nec-1 as in the isatin-only treatment (Fig. 5B). For instance, after 5 h, cells subjected to combination treatment showed an average area of 200 μm^2 larger than isatin-treated samples. Moreover, at long term time points, only isatin **1** had similar values in combinatory and single treatments. A similar feature is observed in the evolution of mean dry mass, in which no decrease is observed in any of the treatments except for a subtle reduction after 15 h of exposure to **1**. This difference illustrates the limited necroptosis observed in the population when co-incubated with Nec-1. In the case of form factor and compactness, the trends observed in the individual treatments were present also in the co-incubated samples but in a more modest way, probably due to the morphological changes were not extended in the population. These results suggested that the cell death induced by the isatin derivatives is not an indiscriminate necrosis but a regulated form of cell death that matches with necroptotic cell death.

4. Discussion

The isatin scaffold in chemical entities has been explored for antimigratory, antiproliferative and pro-apoptotic agents [10,12]. In general terms, the potency of these structures is modest, with a relatively high GI_{50} (50–200 μM). Hence, their chances to be used as antineoplastic drugs are reduced since the high amount of drug needed increase the probability of side effects due to promiscuous interactions or off-site targeting. We reported earlier that isatins bearing a halomethylene groups displayed an enhanced potency against tumor cells, achieving effects at the nanomolar range [7]. The activity is not only limited to cytotoxicity since these compounds also produced an inhibition of the migratory ability of NSCLC A549 cell line (Fig. 3). Moreover, more insight into the SAR could be established, since the halogen substituted compounds at the phenyl ring **1** and **3** were the ones that presented better results. The inclusion of halogens for more efficient activity was also described in the past. Structural requirements for the antiproliferative activity of modified isatins has been well described through QSAR methods [30]. Different halogen substituted isatins have been reported as molecules with anticancer properties like histone deacetylase inhibitors [31] or selective carbonic anhydrase inhibitors [32]. Sunitinib (Fig. 1) –an isatin-based compound containing a fluorine– was approved for clinical treatment of renal cell carcinoma during the last decade, although with limited efficacy [33].

For the set of isatin derivatives studied in this work, necrosis was the predominant mode of cell death with cell line specificity over two different NSCLC tumor cell lines. Exposure to **1**–**3** had a significant impact on SW1573 cells at a lower concentration compared to that used for A549 cells, where the effect was less pronounced. The discrepancy in the GI_{50} values after 48 h of exposure varied by a substantial factor, ranging from 300 to 500 times between the two cell lines. (Table 1).

Our initial proposed interaction between the isatin derivatives **1**–**3** and the protein variant KRAS G12C was discarded after in silico studies.

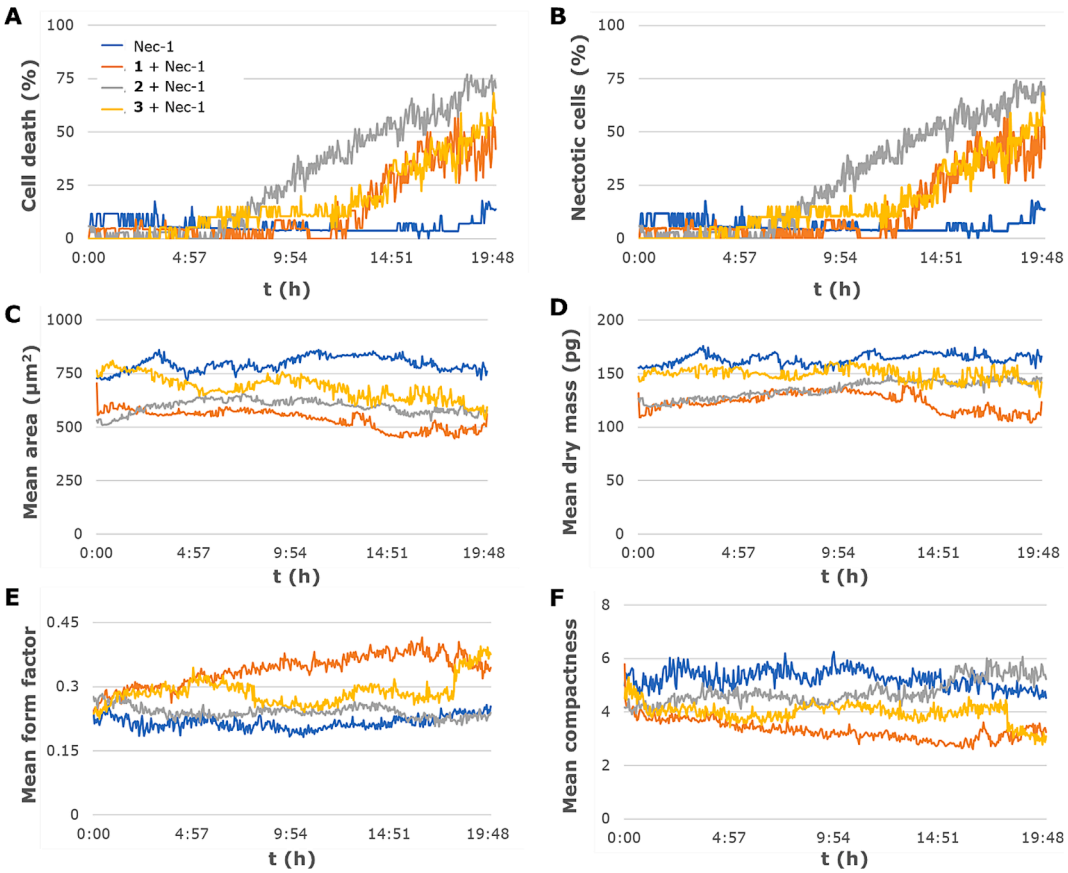

Fig. 12. Kinetics of the cell death (%) and RI-based parameters for the population of SW1573 cells preincubated with Nec-1 for 30 min and treated with the isatin derivatives **1**–**3** for 20 h.

This result might be related for two reasons. On the one hand, the nucleophilic substitution that should takes place between the Cys12 and the chloromethylene residue is not possible. On the other hand, there is no interaction between the isatin candidates **1**–**3** and the KRAS G12C protein. GPX4 inhibitors RSL3 and ML162 bind GPX4 covalently via the chloroacetamide moiety [34]. However, the amino acid residue reacting with the chloroacetamide fragment is selenocysteine (Sec), also known as the 21st amino acid. Sec has electronic properties different from Cys, which makes it suitable to undergo the nucleophilic substitution, supporting the first argument. In such case, we speculate that the significant sensitivity to KRAS G12C cells might be due to the interaction with molecular targets other than KRAS. This is supported by the antiproliferative results observed for KRAS mutant cell lines (Table 1).

Regarding the mode of cell death, induction of apoptosis has been observed in several subsets of isatin-derived compounds against different cell lines [35–37]. Although necrotic cell death has also been reported, these examples are just mainly limited to late apoptosis that has transitioned to necrosis as a consequence of the use of high concentrations of the drugs [38,39]. Continuous live cell imaging allowed to identify necrotic phenotypes through the observation of cell swelling, loss of cellular membrane, leakage of cell content to the extracellular environment and rounded and reduced nuclear size without cell shrinkage. The use of fluorescent dyes confirmed some of these features. DAPI staining demonstrated the loss of nuclear structures and the reduction in DNA content, meanwhile positive PI staining marked the loss of membrane integrity, confirming the necrosis as the mode of cell death (Fig. 8). Live cell staining with Hoechst 33,342 supported these results, highlighting that some of these features occurred before 5 h of exposure (Fig. 10). The continuous observation of the cell responses to treatment also showed an increase of Hoechst fluorescent signal during cell size reduction without the presence of apoptotic phenotypes. This cell permeable dye binds to the adenine–thymine regions in the DNA minor groove. Thus, decrease of fluorescent signal could point out drug induced DNA damage. Indeed, the isatin derivatives **1**–**3** are far from producing a promiscuous response since it has been demonstrated that their potency is cell line dependent. Extensive necrotic cell death is induced in SW1573 cells before 5 h of exposure when using doses that barely affected another cell line from a related tissue (Fig. 5).

Traditionally, the induction of necrosis by anticancer compounds has been considered as an undesired event in the development of new drugs as it is an uncontrolled way leading to cell death, generally related to extreme conditions that could damage healthy tissues producing important side effects. However, triggering a regulated form of necrosis, i.e. necroptosis, has been described recently as an efficient MoA of some new anticancer drugs [40,41]. This novel paradigm for cytotoxic induction opened the door for alternative ways that could overcome resistance. Adaptive mechanisms in the regulation of the apoptotic machinery have compromised the efficacy of validated drugs in the treatment of cancer, resulting in therapeutic resistance to pro-apoptotic agents [42]. Several types of tumors are able to induce the expression of antiapoptotic proteins such as Bcl-2, Bcl-xL and survivin whilst decreasing pro-apoptotic signals driven by bax, bak, bim or puma, among others. These mechanisms of resistance can occur both intracellularly and communicatively between the population, transforming adjacent cells through paracrine signaling [28]. Therefore, the ability to induce a controlled form of necrotic cell death represents a new strategy for cancer treatment [43]. Remarkably, the pre-incubation of SW1573 cells with a necroptosis inhibitor reduced drastically cell death produced by the isatin derivatives (Fig. 11), pointing out that the necrotic phenotypes observed are not the result of an uncontrolled event caused by unspecific damage but a mode of regulated cell death. It remains unclear whether there is a relationship or not between necroptosis observed in

SW1573 cells and the KRAS status of the cell line. In this particular context, the literature does not inform of necroptosis for the KRAS (G12C) inhibitors AMG510 (sotorasib) and MRTX849 (adagrasib). Taking as a whole this fact and our observations reported herein, isatin derivatives **1**–**3** are not likely to behave as KRAS substrates. In essence, necroptosis induced by isatin derivatives **1**–**3** should be studied in more detail to unveil the molecular target.

5. Conclusions

In this work, we have explored in detail the mode of action of a set of isatin derivatives selected from a preliminary screening of a 38 compound library. With the aid of phenotypic assays, we could establish some activity profiling of the compounds related to their pharmacodynamics with a particular focus on the kinetics of cell death. The results allowed us to select compound **1** as the drug lead of the series and to propose necroptosis as the main MoA of the compounds. The cellular target remains unknown and further studies will be necessary to fully unveil the features that confers selectivity towards specific cell lines.

CRediT authorship contribution statement

Adrián Puerta: Writing – original draft, Methodology, Investigation, Formal analysis, Data curation, Conceptualization. **Aday González-Bakker:** Methodology, Investigation, Data curation. **Pedro Brandão:** Resources. **Marta Pineiro:** Resources. **Anthony J. Burke:** Resources. **Elisa Giovannetti:** Resources. **Miguel X. Fernandes:** Software, Investigation, Formal analysis. **José M. Padrón:** Writing – review & editing, Writing – original draft, Supervision, Resources, Project administration, Investigation, Funding acquisition, Conceptualization.

Declaration of competing interest

The authors declare that they have no known competing financial interests or personal relationships that could have appeared to influence the work reported in this paper.

Data availability

Data will be made available on request.

Acknowledgments

A.P., A.G.-B. and J.M.P. thank the Spanish Government (Project PID2021-123059OB-I00 funded by MCIN/AEI /10.13039/501100011033 / FEDER, UE). A.P. thanks the EU Social Fund (FSE) and the Canary Islands ACIISI for a predoctoral grant TESIS2020010055. A. G.-B. thanks the Asociación Española Contra el Cáncer (AECC) de Santa Cruz de Tenerife for a predoctoral grant PRDTF233958GONZ. P.B thanks the Fundação para a Ciência e Tecnologia (FCT) for PhD grant PD/BD/128490/2017-CATSUS FCT-PhD Program and funding in the scope of projects UIDB/04565/2020 and UIDP/04565/2020 of the Research Unit iBB; and LA/P/0140/2020 of the Associate Laboratory i4HB; and UIDB/04585/2020 of the Research Unit Egas Moniz Center for Interdisciplinary Research (CiiEM). P.B. and M.P. thank the FCT through projects UIDB/00313/2020 and UIDP/00313/2020. We thank Dr. Ricardo Reyes (ULL) for the use of the Leica fluorescent microscope.

Appendix A. Supplementary data

Supplementary data to this article can be found online at https://doi.org/10.1016/j.bcp.2024.116059.

References

[1] S. Chowdhary, Shalini, A. Arora, V. Kumar, A mini review on Isatin, an anticancer scaffold with potential activities against neglected tropical diseases (NTDs), Pharmaceuticals 15 (2022) 536, https://doi.org/10.3390/ph15050536.
[2] L.A. Justo, R. Durán, M. Alfonso, D. Fajardo, L.R.F. Faro, Effects and mechanism of action of Isatin, a MAO inhibitor, on in vivo striatal dopamine release, Neurochem. Int. 99 (2016) 147–157, https://doi.org/10.1016/j.neuint.2016.06.012.
[3] P. Pakravan, S. Kashanian, M.M. Khodaei, F.J. Harding, Biochemical and Pharmacological Characterization of Isatin and Its Derivatives: From Structure to Activity, Pharmacol. Rep. 65 (2013) 313–335, https://doi.org/10.1016/s1734-1140(13)71007-7.
[4] R.S. Cheke, V.M. Patil, S.D. Firke, J.P. Ambhore, I.A. Ansari, H.M. Patel, S. D. Shinde, V.R. Pasupuleti, M.I. Hassan, M. Adnan, A. Kadri, M. Snoussi, Therapeutic Outcomes of Isatin and Its Derivatives against Multiple Diseases: Recent Developments in Drug Discovery, Pharmaceuticals 15 (2022) 272, https://doi.org/10.3390/ph15030272.
[5] Z. Ding, M. Zhou, C. Zeng, Recent Advances in Isatin Hybrids as Potential Anticancer Agents, Arch. Pharm. 353 (2020) e1900367.
[6] R.E. Ferraz de Paiva, E.G. Vieira, D. Rodrigues da Silva, C.A. Wegermann, A. M. Costa Ferreira, Anticancer Compounds Based on Isatin-Derivatives: Strategies to Ameliorate Selectivity and Efficiency, Front. Mol. Biosci. 7 (2020) 627272, https://doi.org/10.3389/fmolb.2020.627272.
[7] P. Brandão, A. Puerta, J.M. Padrón, M.L. Kuznetsov, A.J. Burke, M. Pineiro, Ugi Adducts of Isatin as Promising Antiproliferative Agents with Druglike Properties, Asian J. Org. Chem. 10 (12) (2021) 3434–3455, https://doi.org/10.1002/ajoc.202100684.
[8] A.U.M. Khan, A. Torelli, I. Wolf, N. Gretz, AutoCellSeg: robust automatic colony forming unit (CFU)/cell analysis using adaptive image segmentation and easy-to-use post-editing techniques, Sci. Rep. 8 (2018) 7302, https://doi.org/10.1038/s41598-018-24916-9.
[9] P. Xu, L. Hou, C. Ju, Z. Zhang, W. Sun, L. Zhang, J. Song, Y. Lv, L. Liu, Z. Chen, Y. Wang, Isatin Inhibits the Proliferation and Invasion of SH SY5Y Neuroblastoma Cells, Mol. Med. Rep. 13 (3) (2016) 2757–2762, https://doi.org/10.3892/mmr.2019.10378.
[10] W. Sun, L. Zhang, L. Hou, C. Ju, S. Zhao, Y. Wei, Isatin Inhibits SH-SY5Y Neuroblastoma Cell Invasion and Metastasis through MAO/HIF-1α/CXCR4 Signaling, Anticancer Drugs 28 (6) (2017) 645–653, https://doi.org/10.1097/CAD.0000000000000505.
[11] N. Liu, Y. Li, S. Su, N. Wang, H. Wang, J. Li, Inhibition of Cell Migration by Ouabain in the A549 Human Lung Cancer Cell Line, Oncol. Lett. 6 (2013) 475–479, https://doi.org/10.3892/ol.2013.1406.
[12] B. Yu, S.Q. Wang, P.P. Qi, D.X. Yang, K. Tang, H.M. Liu, Design and Synthesis of Isatin/Triazole Conjugates That Induce Apoptosis and Inhibit Migration of MGC-803 Cells, Eur. J. Med. Chem. 124 (2016) 350–360, https://doi.org/10.1016/j.ejmech.2016.08.065.
[13] Q. Gao, W. Ouyang, B. Kang, X. Han, Y. Xiong, R. Ding, Y. Li, F. Wang, L. Huang, L. Chen, D. Wang, X. Dong, Z. Zhang, Y. Li, B. Ze, Y. Hou, H. Yang, Y. Ma, Y. Gu, C.-C. Chao, Selective Targeting of the Oncogenic KRAS G12S Mutant Allele by CRISPR/Cas9 Induces Efficient Tumor Regression, Theranostics 10 (2020) 5137–5153, https://doi.org/10.7150/thno.42325.
[14] S. Misale, J.P. Fatherree, E. Cortez, C. Li, S. Bilton, D. Timonina, D.T. Myers, D. Lee, M. Gomez-Caraballo, M. Greenberg, V. Nangia, P. Greninger, R.K. Egan, J. McClanaghan, G.T. Stein, E. Murchie, P.P. Zarrinkar, M.R. Janes, L.-S. Li, Y. Liu, A.N. Hata, C.H. Benes, KRAS G12C NSCLC Models Are Sensitive to Direct Targeting of KRAS in Combination with PI3K Inhibition, Clin. Cancer Res. 25 (2019) 796–807, https://doi.org/10.1158/1078-0432.CCR-18-0368.
[15] J. Roth, P. Koch, A. Contente, M. Dobbelstein, Tumor-Derived Mutations within the DNA-Binding Domain of P53 That Phenotypically Resemble the Deletion of the Proline-Rich Domain, Oncogene 19 (2000) 1834–1842, https://doi.org/10.1038/sj.onc.1203500.
[16] M.R. Janes, J. Zhang, L.-S. Li, R. Hansen, U. Peters, X. Guo, Y. Chen, A. Babbar, S. J. Firdaus, L. Darjania, J. Feng, J.H. Chen, S. Li, S. Li, Y.O. Long, C. Thach, Y. Liu, A. Zarieh, T. Ely, J.M. Kucharski, L.V. Kessler, T. Wu, K. Yu, Y. Wang, Y. Yao, X. Deng, P.P. Zarrinkar, D. Brehmer, D. Dhanak, M.V. Lorenzi, D. Hu-Lowe, M. P. Patricelli, P. Ren, Y. Liu, Targeting KRAS Mutant Cancers with a Covalent G12C-Specific Inhibitor, Cell 172 (2018) 578–589.e17, https://doi.org/10.1016/j.cell.2018.01.006.
[17] S. Kim, N. Kim, K. Kang, W. Kim, J. Won, J. Cho, Whole Transcriptome Analysis Identifies TNS4 as a Key Effector of Cetuximab and a Regulator of the Oncogenic Activity of KRAS Mutant Colorectal Cancer Cell Lines, Cells 8 (2019) 878, https://doi.org/10.3390/cells8080878.
[18] B.L. Grigorenko, A.V. Nemukhin, M.S. Shadrina, I.A. Topol, S.K. Burt, Mechanisms of Guanosine Triphosphate Hydrolysis by Ras and Ras-GAP Proteins as Rationalized by Ab Initio QM/MM Simulations, Proteins 66 (2007) 456–466, https://doi.org/10.1002/prot.21228.
[19] D.K. Menyhárd, G. Pálfy, Z. Orgován, I. Vida, G.M. Keserű, A. Perczel, Structural impact of GTP binding on downstream KRAS signaling, Chem. Sci. 11 (2020) 9272–9289, https://doi.org/10.1039/d0sc03441j.
[20] B.A. Lanman, J.R. Allen, J.G. Allen, A.K. Amegadzie, K.S. Ashton, S.K. Booker, J. J. Chen, N. Chen, M.J. Frohn, G. Goodman, D.J. Kopecky, L. Liu, P. Lopez, J. D. Low, V. Ma, A.E. Minatti, T.T. Nguyen, N. Nishimura, A.J. Pickrell, A.B. Reed, Y. Shin, A.C. Siegmund, N.A. Tamayo, C.M. Tegley, M.C. Walton, H.L. Wang, R. P. Wurz, M. Xue, K.C. Yang, P. Achanta, M.D. Bartberger, J. Canon, L.S. Hollis, J. D. McCarter, C. Mohr, K. Rex, A.Y. Saiki, T. San Miguel, L.P. Volak, K.H. Wang, D. A. Whittington, S.G. Zech, J.R. Lipford, V.J. Cee, Discovery of a Covalent Inhibitor

of KRASG12C (AMG 510) for the Treatment of Solid Tumors, J. Med. Chem. 63 (2020) 52–65, https://doi.org/10.1021/acs.jmedchem.9b01180.
[21] J.C. Hunter, A. Manandhar, M.A. Carrasco, D. Gurbani, S. Gondi, K.D. Westover, Biochemical and Structural Analysis of Common Cancer-Associated KRAS Mutations, Mol. Cancer Res. 13 (2015) 1325–1335, https://doi.org/10.1158/1541-7786.
[22] P.A. Jänne, G.J. Riely, S.M. Gadgeel, R.S. Heist, S.-H.-I. Ou, J.M. Pacheco, M. L. Johnson, J.K. Sabari, K. Leventakos, E. Yau, L. Bazhenova, M.V. Negrao, N. A. Pennell, J. Zhang, K. Anderes, H. Der-Torossian, T. Kheoh, K. Velastegui, X. Yan, J.G. Christensen, R.C. Chao, A.I. Spira, Adagrasib in Non–Small-Cell Lung Cancer Harboring a KRASG12C Mutation, New Eng J Med 387 (2022) 120–131, https://doi.org/10.1056/NEJMoa2204619.
[23] G. Fan, L. Lou, Z. Song, X. Zhang, X.-F. Xiong, Targeting Mutated GTPase KRAS in Tumor Therapies, Eur. J. Med. Chem. 226 (2021) 113816, https://doi.org/10.1016/j.ejmech.2021.113816.
[24] J. Kapuscinski, DAPI: a DNA-specific fluorescent probe, Biotech. Histochem. 70 (1995) 220–233, https://doi.org/10.3109/10520299509108199.
[25] L.C. Crowley, A.P. Scott, B.J. Marfell, J.A. Boughaba, G. Chojnowski, N. J. Waterhouse, Measuring cell death by propidium iodide uptake and flow cytometry, Cold Spring Harb. Protoc. 2016 (7) (2016), https://doi.org/10.1101/pdb.prot087163.
[26] T. Vanden Berghe, N. Vanlangenakker, E. Parthoens, W. Deckers, M. Devos, N. Festjens, C.J. Guerin, U.T. Brunk, W. Declercq, P. Vandenabeele, Necroptosis, Necrosis and Secondary Necrosis Converge on Similar Cellular Disintegration Features, Cell Death Differ. 17 (2010) 922–930, https://doi.org/10.1038/cdd.2009.184.
[27] P. Golstein, G. Kroemer, Cell Death by Necrosis: Towards a Molecular Definition, Trends Biochem. Sci. 32 (2007) 37–43, https://doi.org/10.1016/j.tibs.2006.11.001.
[28] Y. Woo, H.-J. Lee, Y.M. Jung, Y.-J. Jung, Regulated Necrotic Cell Death in Alternative Tumor Therapeutic Strategies, Cells 9 (2020) 2709, https://doi.org/10.3390/cells9122709.
[29] L. Cao, W. Mu, Necrostatin-1 and Necroptosis Inhibition: Pathophysiology and Therapeutic Implications, Pharmacol. Res. 163 (2021) 105297, https://doi.org/10.1016/j.phrs.2020.105297.
[30] R. Sabet, M. Mohammadpour, A. Sadeghi, A. Fassihi, QSAR Study of Isatin Analogues as in Vitro Anti-Cancer Agents, Eur. J. Med. Chem. 45 (2010) 1113–1118, https://doi.org/10.1016/j.ejmech.2009.12.010.
[31] A. Singh, K. Raghuwanshi, V.K. Patel, D.K. Jain, R. Veerasamy, A. Dixit, H. Rajak, Assessment of 5-Substituted Isatin as Surface Recognition Group: Design, Synthesis, and Antiproliferative Evaluation of Hydroxamates as Novel Histone Deacetylase Inhibitors, Pharm. Chem. J. 51 (2017) 366–374, https://doi.org/10.1007/s11094-017-1616-1.
[32] W.M. Eldehna, M. Fares, M. Ceruso, H.A. Ghabbour, S.M. Abou-Seri, H.A. Abdel-Aziz, D.A. Abou El Ella, C.T. Supuran, Amido/Ureidosubstituted Benzenesulfonamides-Isatin Conjugates as Low Nanomolar/Subnanomolar Inhibitors of the Tumor-Associated Carbonic Anhydrase Isoform XII, Eur. J. Med. Chem. 110 (2016) 259–266, https://doi.org/10.1016/j.ejmech.2016.01.030.
[33] S. Astore, G. Baciarello, L. Cerbone, F. Calabrò, Primary and Acquired Resistance to First-Line Therapy for Clear Cell Renal Cell Carcinoma, Cancer Drug Resist. 6 (2023) 517–546, https://doi.org/10.20517/cdr.2023.33.
[34] L. Wang, X. Chen, C. Yan, Ferroptosis: An Emerging Therapeutic Opportunity for Cancer, Genes Dis. 9 (2022) 334–346, https://doi.org/10.1016/j.gendis.2020.09.005.
[35] J. Song, L. Hou, C. Ju, J. Zhang, Y. Ge, W. Yue, Isatin Inhibits Proliferation and Induces Apoptosis of SH-SY5Y Neuroblastoma Cells in Vitro and in Vivo, Eur. J. Pharmacol. 702 (2013) 235–241, https://doi.org/10.1016/j.ejphar.2013.01.017.
[36] S. Kour, S. Rana, S.P. Kubica, S. Kizhake, M. Ahmad, C. Muñoz-Trujillo, D. Klinkebiel, S. Singh, J.R. Mallareddy, S. Chandra, N.T. Woods, A.R. Karpf, A. Natarajan, Spirocyclic Dimer SpiD7 Activates the Unfolded Protein Response to Selectively Inhibit Growth and Induce Apoptosis of Cancer Cells, J. Biol. Chem. 298 (2022) 101890, https://doi.org/10.1016/j.jbc.2022.101890.
[37] W.M. Eldehna, R. Salem, Z.M. Elsayed, T. Al-Warhi, H.R. Knany, R.R. Ayyad, T. B. Traiki, M.-H. Abdulla, R. Ahmad, H.A. Abdel-Aziz, R. El-Haggar, Development of Novel Benzofuran-Isatin Conjugates as Potential Antiproliferative Agents with Apoptosis Inducing Mechanism in Colon Cancer, J. Enzyme Inhib. Med. Chem. 36 (2021) 1424–1435, https://doi.org/10.1080/14756366.2021.1944127.
[38] M.-A. Vaali-Mohammed, M.-H. Abdulla, S. Matou-Nasri, W.M. Eldehna, M. Meeramaideen, E.B. Elkaeed, M. El-Watidy, N.S. Alhassan, K. Alkhaya, O. Al Obeed, The Anticancer Effects of the Pro-Apoptotic Benzofuran-Isatin Conjugate (5a) Are Associated With P53 Upregulation and Enhancement of Conventional Chemotherapeutic Drug Efficiency in Colorectal Cancer Cell Lines, Front. Pharmacol. 13 (2022) 923398, https://doi.org/10.3389/fphar.2022.923398.
[39] N. Igosheva, C. Lorz, E. O'Conner, V. Glover, H. Mehmet, Isatin, an Endogenous Monoamine Oxidase Inhibitor, Triggers a Dose- and Time-Dependent Switch from Apoptosis to Necrosis in Human Neuroblastoma Cells, Neurochem. Int. 47 (2005) 216–224, https://doi.org/10.1016/j.neuint.2005.02.011.
[40] S.A. Saddoughi, S. Gencer, Y.K. Peterson, K.E. Ward, A. Mukhopadhyay, J. Oaks, J. Bielawski, Z.M. Szulc, R.J. Thomas, S.P. Selvam, C.E. Senkal, E. Garrett-Mayer, R.M. De Palma, D. Fedarovich, A. Liu, A.A. Habib, R.V. Stahelin, D. Perrotti, B. Ogretmen, Sphingosine Analogue Drug FTY720 Targets I2PP2A/SET and Mediates Lung Tumour Suppression via Activation of PP2A-RIPK1-Dependent Necroptosis, EMBO Mol. Med. 5 (2013) 105–121, https://doi.org/10.1002/emmm.201201283.
[41] J.H. Park, K.H. Jung, S.J. Kim, Y.-C. Yoon, H.H. Yan, Z. Fang, J.E. Lee, J.H. Lim, S. Mah, S. Hong, Y.-S. Kim, S.-S. Hong, HS-173 as a Novel Inducer of RIP3-Dependent Necroptosis in Lung Cancer, Cancer Lett. 444 (2019) 94–104, https://doi.org/10.1016/j.canlet.2018.12.006.
[42] C. Ríos-Luci, E. Díaz-Rodríguez, L. Gandullo-Sánchez, L. Díaz-Gil, A. Ocaña, A. Pandiella, Adaptive resistance to trastuzumab impairs response to neratinib and lapatinib through deregulation of cell death mechanisms, Cancer Lett. 470 (2020) 161–169, https://doi.org/10.1016/j.canlet.2019.11.026.
[43] Z. Su, Z. Yang, L. Xie, J.P. DeWitt, Y. Chen, Cancer Therapy in the Necroptosis Era, Cell Death Differ. 23 (2016) 748–756, https://doi.org/10.1038/cdd.2016.8.